LIQUID DIFFRACTION ANALYSIS OF THE MODEL MEMBRANE SYSTEM

EGG LECITHIN + MYELIN PROTEIN (N-2)

G. W. BRADY AND P. S. BIRNBAUM, *Division of Laboratories and Research, New York State Department of Health, Albany, New York 12201 and Department of Physics and Center for Biological Macromolecules, State University of New York at Albany, New York 12222*

M. A. MOSCARELLO, *Department of Biochemistry, Research Institute, Hospital for Sick Children, Toronto, Ontario, Canada*

D. PAPAHADJOPOULOS, *Department of Experimental Pathology, Roswell Park Memorial Hospital, Buffalo, New York 14263 U.S.A.*

ABSTRACT The scattering from the model membrane system, egg lecithin + myelin protein (N-2), has been analyzed by liquid diffraction methods. It is found that by manipulating the protein-lipid ratio, the scattering domains of the protein and lipid can be identified. The multilayer contribution can also be identified by its position and concentration behavior in both the intensity pattern and its Fourier transform. When the multilayer and protein components are subtracted, the phospholipid scattering and an interaction term are left; these two can be resolved by a reasonable assessment of their relative magnitude in the boundary region where they overlap. The interaction term can then be used to determine the most probable position of the protein in the membrane. The deconvoluted protein and lipid transforms can then be combined in the proper way to obtain the electron density profiles. The resolution of the interaction term is not yet complete, but a method for accomplishing this is discussed.

INTRODUCTION

The analysis of the X-ray diffraction patterns from membranes has had limited success in providing a satisfactory physical picture of their structure. It was recognized quite early (Schmitt et al., 1935; Shipley 1973; Wilkins and Blaurock, 1971) that the phospholipid bilayer was an essential component in the structure, and the development of phasing and deconvolution techniques (Shipley 1973; Wilkins and Blaurock, 1971; Worthington and Blaurock, 1968; Worthington and McIntosh, 1974; Lesslauer and Blasie, 1972; Hosemann and Bagchi, 1962) to deal with the scattering resulted in a model for the electron density profile of the bilayer in satisfactory agreement with that derived from other techniques, such as that of electron microscopy (Fernandez-Moran, 1962; Robertson, 1967). The difficulty arose when the techniques used to analyze the scattering were applied to membranes that

This paper was part of the Symposium on Interactions between Membrane Components, organized by Stephen H. White, held at the Annual Meeting of the Biophysical Society on 26 March 1978.

contained protein. It was found that the presence of proteins had little effect, or at least an ambiguous effect, on the derived electron density profiles (Engleman, 1971; Blaurock and Stockenius, 1971; Caspar and Kirschner, 1971); this led to a rationalization of the results to indicate that the protein formed a layer bound to the membrane surface; in some cases partial penetration into the bilayer interior was suggested. However, the evolution of the freeze-fracture techniques (Branton, 1963; Ruben et al., 1976) of electron microscopy showed, rather inexplicably with respect to the diffraction results, that there was clear evidence for protein particles situated at the interior of the phospholipid bilayer, or at least partially imbedded in it. Later diffraction experiments with oriented membranes by Henderson (1975), Blaurock (1975), and also by Blasie and co-workers (1977) showed the presence of scattering consistent with the presence of α-helical repeat distances in a direction normal to and extending through the bilayers.

This state of affairs has motivated us to undertake a study of the diffraction from protein-

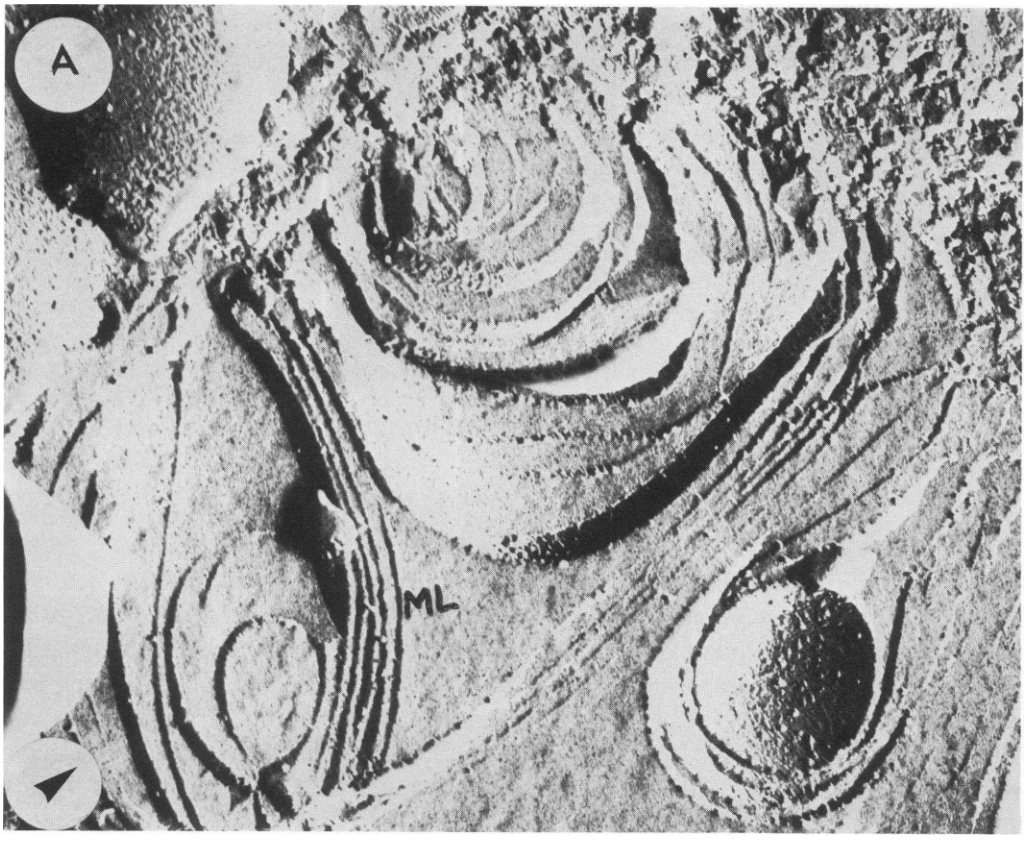

FIGURE 1 Freeze-fracture electron micrographs of liposomes composed of phosphatidylcholine and lipophilin. (A) 10% protein; ML denotes region of multilayer formation; total magnification ×78,000. (B) 50% protein; large craters and hills show single bilayer membranes; small spheres are protein molecules; total magnification ×130,000. Arrow marks direction of shadow. (Photographs courtesy W. J. Vail, Guelph, Ontario.)

containing phospholipid bilayers in which it is known that the protein exists in the interior of the bilayer. Instead of using crystallographic techniques, where phasing or deconvolution of the patterns are attempted on the basis of an assigned background, and reasonable assumptions as to symmetry, we treat the scattering as arising from a liquid system and apply liquid scattering techniques to the data analysis. First principles argue well for this approach, because membranes give liquid-like diffraction patterns, and in other respects exhibit properties consistent with those to be expected from a solution of protein and phospholipid, with limited long-range order (Vanderkooi and Green, 1970; White et al., 1976). In contrast, crystallographic techniques are based on the assumption that the components join together into an array homogenous and regular enough to give patterns that can be characterized by a (± 1) phase sequence common to both components. The advantages of the liquid approach are that no background is assumed and thus all the data can be processed, and in principle the individual components of the scattering, that is the protein, the lipid, and their correlation terms, can be isolated from the others and analyzed separately.

The system chosen for study was egg lecithin, into which was incorporated hydrophobic (N-2) myelin protein in varying concentrations. This protein is at least 60% hydrophobic (Papahadjopoulos et al., 1975*a*) and is completely insoluble in an external aqueous phase. The system itself has been well characterized chemically (Papahadjopoulos et al., 1975*a*),

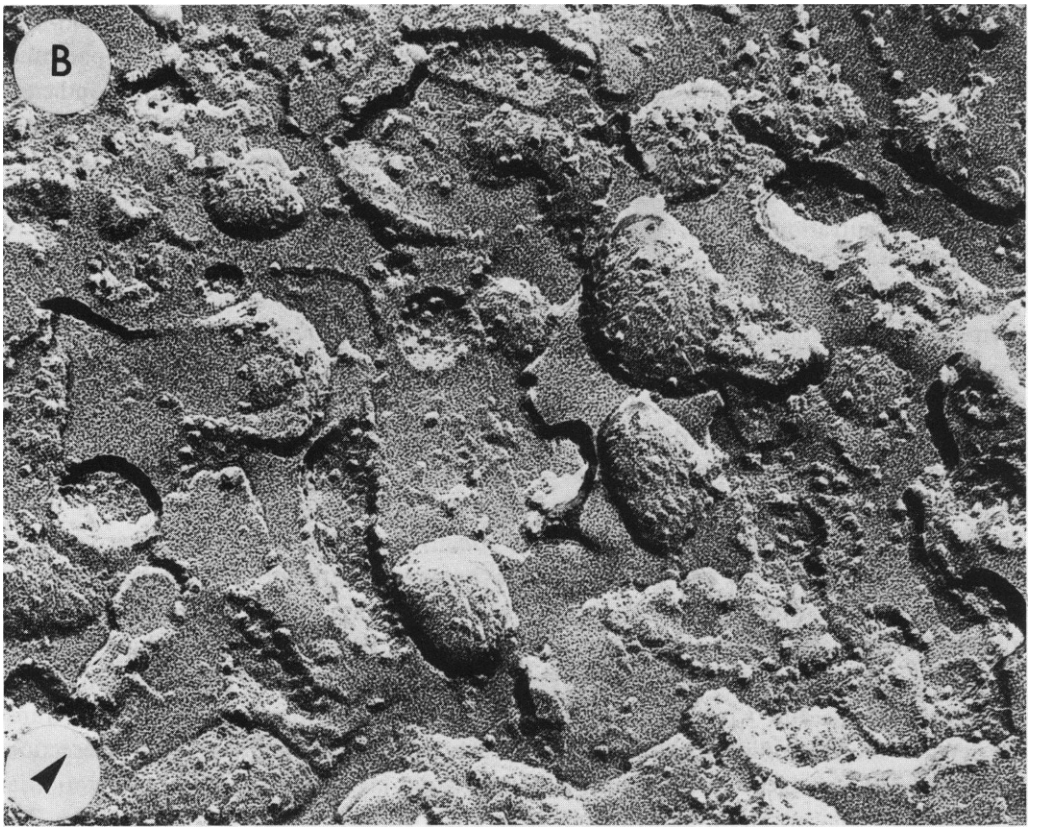

and extensive physical measurements, among them electron spin resonance TEMPO (Boggs et al., 1976) and calorimetric studies (Papahadjopoulos et al., 1975*b*) have been made. The presence of the protein in the interior of the bilayer can be clearly seen in freeze-fracture electron micrographs (Fig. 1).

The description that follows shows that the technique developed is quite successful in analyzing the scattering, and although some refinement in the evaluation of the lipid-protein correlation term is desirable, the results in their present state are worth publishing. The procedure is equally applicable to natural membrane.

ANALYSIS

The scattering from the two component membrane liquid systems can be written as

$$\begin{aligned} I &= (I_{\text{prot}} + I_{\text{lip}} + I_{\text{pl}})_B + I_m \\ &= x\phi_{\text{prot}}^2 + (1 - x)\phi_{\text{lip}}^2 + 2x(1 - x)\phi_{\text{prot}}\phi_{\text{lip}}C'(r), \end{aligned} \tag{1}$$

where ϕ_{prot} and ϕ_{lip} are the structure factors of the protein and phospholipid components, x and $(1 - x)$ are their respective mole fractions, and $C'(r)$ is the Fourier transform of a correlation term that expresses the spatial organization of the protein and phospholipid with respect to each other. Corresponding $C(r)$'s exist for protein-protein and lipid-lipid correlations, but for the present these are included in the respective ϕ^2's. The parenthesis subscript B indicates that the terms in it refer to a bilayer. The term I_m indicates multilayer scattering; it is necessary to include this term because, as will be seen later, the system exists in multilayer form at zero protein concentration and in single bilayer form at high ($\sim 50\%$) protein concentration, with gradations between these two forms at the intermediate concentrations.

In a simple binary system, characterized by two invariant scattering factors, the application of this equation is generally straightforward, and it is possible to evaluate the individual terms in it (Brady and Kaplan, 1973; Brady, 1971, 1974). When applied to a membrane system, the main complication arises in the evaluation of ϕ_{lip}^2. The bilayer is a highly organized structure when present alone, and it can be foreseen that the introduction of protein will seriously affect this structure with the formation of regions of phospholipid, whose structure factors will not necessarily be submultiples of those appropriate to the continuous bilayer; in fact, there is no way a priori of telling how the bilayer structure is modified. Thus, the second and third terms in Eq. 1 will not be directly separable by studying their variation with respect to x, since ϕ_{lip} and ϕ_{lip}^2 will also be changing. On the other hand, ϕ_{prot}^2 does not change with concentration, or does so in a measurable way, so the I_{prot} can be evaluated directly; the concentration dependence of the I_m term, and thus its contribution to the scattering, can also be determined. Thus, the successful application of Eq. 1 rests on a valid separation of I_{lip} and I_{pl}. This can be accomplished by utilization of Fourier transform methods, which allow identification of the electron pairs belonging to each interaction, and from a knowledge of the amount of phospholipid arranged in parallel orientation at each protein concentration, gained from wide angle studies (Brady & Fein, 1979). The

isolated protein and phospholipid terms can be deconvoluted, then combined in a proper way to synthesize the final structure.

X-RAY MEASUREMENTS AND DATA PROCESSING

The data were measured with a Kratky camera (Anton Paar KG, Graz, Austria), by using CuKα (λ = 1.54 A) radiation, and collected in a PDP8/E on-line computer (Digital Equipment Corp., Maynard, Mass.). The patterns were step-scanned at intervals of $\Delta s = 2 \times 10^{-3}$ Å^{-1} between $s = 0.010$ and $s = 0.65$; the probable error per point was 1.2%. The data were averaged over a seven-point interval by a least-squares program to give an estimated accuracy of 0.5%. The scans were programmed so that different parts of the pattern were taken at different times with sufficient overlap of the parts to ensure that no long-term drift took place, or that no settling of the suspensions occurred. The background used was that of the cell filled with buffer. After correction for absorption, it was subtracted from the measured curves to obtain the corrected patterns. These operations were done on-line and each step could be monitored by a printout or an oscilloscope display. The patterns were then desmeared by using the program of Schmidt and Hight (1960). The pattern for the pure lecithin was characterized by three reflections too sharp and intense, relative to the rest of the pattern, for the program to handle adequately. This was manifested by an overcorrection of the first two peaks, with the appearance of significant negative values at the low angle side of the first one. Although the curve is shown in Fig. 2, it was not considered in the subsequent analysis.

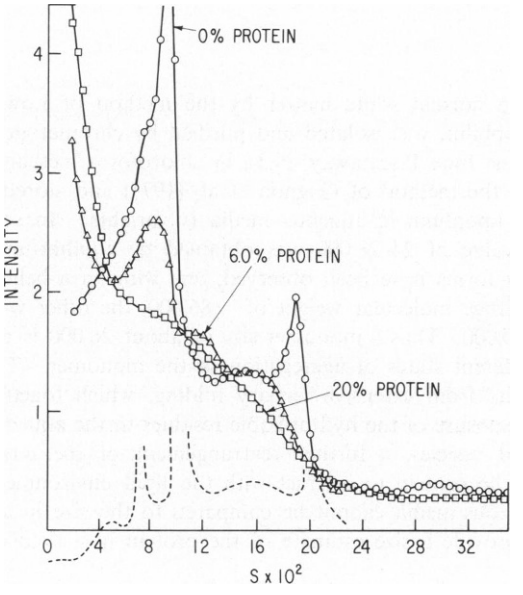

FIGURE 2 Smeared curves for three protein concentrations. The 0% curve has three reflections superimposed on the continuous curve, indicating that some of the material is in a highly ordered phase. The curves have not been corrected for variations (±15%) in concentration and are thus not quantitatively comparable. The dashed curve results when the 0% curve is desmeared (see text). Its ordinate scale is 3 times other curves.

The Fourier transforms were evaluated by computer integration of the equation (Brady and Krause, 1957; Brady 1960):

$$r\tilde{\rho}^2 = rD_{ij}(r) = (1/2\pi^2) \int_0^\infty sI(s) \sin rs \, ds, \tag{2}$$

where $D_{ij}(r)$ is the sum of the electron pair distributions for each type of interaction, with $i = j$ and $i \neq j$, and $I(s)$ is the measured intensity, corrected for background, slit smearing, and adsorption; $s = (4\pi/\lambda) \sin \theta$ is the scattering variable, where λ is the wavelength of the incident radiation and θ is one-half the scattering angle. A fast Fourier transform or Simpson's rule algorithm was used for the integration. With the number of experimental points used, the error was less than 1%.

Where appropriate, the transforms were deconvoluted to give the electron densities. This operation is essentially the solution of the differential equation

$$\tilde{\rho}^2(y) = \int_{-\infty}^{+\infty} \rho(t)\rho(t - y) \, dt. \tag{3}$$

(The equation is of course only applicable to the symmetrical components of the transforms.) A modification of the Pape procedure (Pape et al., 1974) was used for this purpose, in combination with a double sum algorithm that convoluted back the result of the deconvolution to reproduce the original transform. In this way, computer rounding errors and minor experimental errors were minimized (Lesslauer and Blasie, 1972).

We will elaborate on these operations during the course of the discussion.

MATERIALS

Myelin was isolated from normal white matter by the method of Lowden et al., (1966); (N-2) myelin protein, called lipophilin, was isolated and purified by chromatography in Sephadex LH-20 (Pharmacia Fine Chemicals Inc., Piscataway, N.J.) in chloroform/methanol (1:1, vol/vol) containing 5% of 0.1 N HCl, by the method of Gagnon et al. (1971) and stored in the lyophilized form. The molecular weight of lipophilin in aqueous media is variable. In sodium dodecyl sulfate or formic acid solutions a value of 24–28,000 was obtained by equilibrium ultracentrifugation. In H_2O, two conformational forms have been observed, one with an α-helical content of ~50% and an equilibrium ultracentrifuge molecular weight of ~86,000, the other with a β-conformation and a molecular weight of 500,000. Thus a monomer size of about 26,000 is indicated. The other two forms must represent different states of aggregation of the monomer. The tendency to aggregate in aqueous solution results from extensive tertiary folding, which together with subunit association, tends to minimize exposure of the hydrophobic residues to the aqueous phase. On incorporation of protein into lipid vesicles, a further rearrangement of the tertiary structure occurs to allow some segments of the protein to interact with the lipid environment. For this reason the size of the protein in aqueous media cannot be compared to the size in a lipid environment. The present data (see later) provide a size estimate of the protein in a lipid environment for the first time.

Egg lecithin of high purity, as determined by thin-layer chromatography, was dissolved in a small volume of 90% 2-chloroethanol (2 mg lipid/0.4 ml solvent). The dry protein was dissolved in 90% 2-chloroethanol at a concentration of 5 mg/ml and sonicated briefly with a probe sonicator. The two solutions were combined in the desired ratios and were dialyzed against 2 liters buffer containing NaCl (10 mM), histidine (2 mM), *N*-2-hydroxyethylpiperazine-*N'*-2-ethanic sulfonic acid (2 mM), and $CaCl_2$ (1 mM) or EDTA (0.1 mM) adjusted to pH 7.4. The dialysis was carried out at

4°C for 18 h with two changes of buffer. The resulting suspensions were then centrifuged at 105,000 *g* for 3 h on a sucrose gradient. A single, well-defined band was obtained, and the unincorporated protein went to the bottom of the tube. The band was isolated and used to make up the X-ray samples. Samples for freeze-fracture electron micrographs were also prepared. The appearance of only one band indicated the presence of only one species and the micrographs showed the characteristic membrane features. The samples were analyzed for total weight of suspension, and for percentage of protein and phospholipid, by amino acid analysis on a Technicon TSM amino acid analyzer (Technicon Instruments Corp., Tarrytown, N.Y.), and by phosphorous assay according to a modified Bartlett (1959) procedure. The concentrations were in the range of 30–40% mg/ml of suspended membrane material, and the scattering curves were all scaled to the total concentrations of the 35% curve. The experimental temperature was 23°C. The protein concentrations and scattering units for the five systems were: (1) 6.0% ($prot_{0.060} \cdot lip_{0.940}$); (2) 10.2% ($prot_{0.102} \cdot lip_{0.898}$); (3) 15.2% ($prot_{0.152} \cdot lip_{0.848}$); (4) 21.0% ($prot_{0.210} \cdot lip_{0.790}$); (5) 35% ($prot_{0.35} \cdot lip_{0.650}$).

RESULTS AND DISCUSSION

Fig. 1 shows freeze-fracture electron micrographs of the membrane system for a low (5–10%) and high (≥ 50%) protein concentration. The point to note in the low protein micrograph is the presence of regions where well-defined multilayer patterns are observed. The proteins are the small spherical particles which appear in the fracture plane through the bilayer center. The estimated diameter of the proteins is 90–110 Å. These particles are not present in the micrograph of the pure phospholipid. At the high protein concentration all traces of a multilayer pattern have disappeared and the membrane appears as single vesicles with a diameter of ~2,000 Å. The number of protein particles in the fracture plane has increased.

Fig. 2 shows smeared curves for three of the measured concentrations; Fig. 3 shows a comparison between smeared and unsmeared data for the 6.0% curve. In Fig. 2 the pure phospholipid shows three sharp reflections superimposed on a continuous curve. The most intense of these shows a shoulder on the left-hand side, indicating the presence of the maxima,

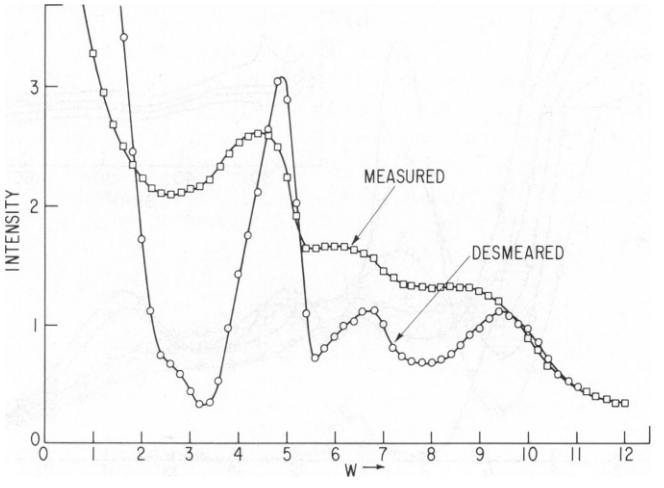

FIGURE 3 Smeared and desmeared data (5% protein). The abscissa is the dial reading of the Kratky camera.

which may be due to the presence of two different chains; egg lecithin is composed mainly of palmitoyl and oleoyl chains. At the lowest protein concentration, two of the three sharp reflections, those at the higher angles, have disappeared.

The unsmeared curves for all concentrations are shown in Fig. 4. Here, it can be seen that the inner reflection, at $s = 0.09$, has given way to a peak that decreases markedly in area and broadens with increasing protein, until at concentrations above 20%, it is no longer clearly evident. This is surely the multilayer component, and its decreases with increasing protein parallel exactly the transformation from a multilayer to a single bilayer, seen in the electron micrographs. The phenomenon is even more clearly demonstrated in the Fourier transform curves, as will be seen later. In Fig. 4 the left-hand side of the multilayer peak is resolved at the lower concentrations. The right-hand side is not resolved over its whole range, but is sufficiently so to allow the rest of the peak to be drawn in by extrapolation. Transformation of the curves with and without the peak included then separates the electron pair distribution into its bilayer and multilayer components.

Protein-lipid interaction effects are first manifested by the appearance of a peak at $s \simeq 0.125$. It is well resolved in the 6 and 10% curve, being slightly broadened at the 10% concentration. It is still evident in the 15% protein curve, but accompanied by other features that become more prominent and eventually obscure it. One of these, evident at the three highest concentrations, is the gradual filling in of the minimum at $s \simeq 0.06$.

The most striking effect of protein addition, however, is the marked increase in scattering at the lowest angles. The pure phospholipid exhibits little if any scattering in the region. This is evident even in the smeared curve that shows a decrease towards zero angle. This

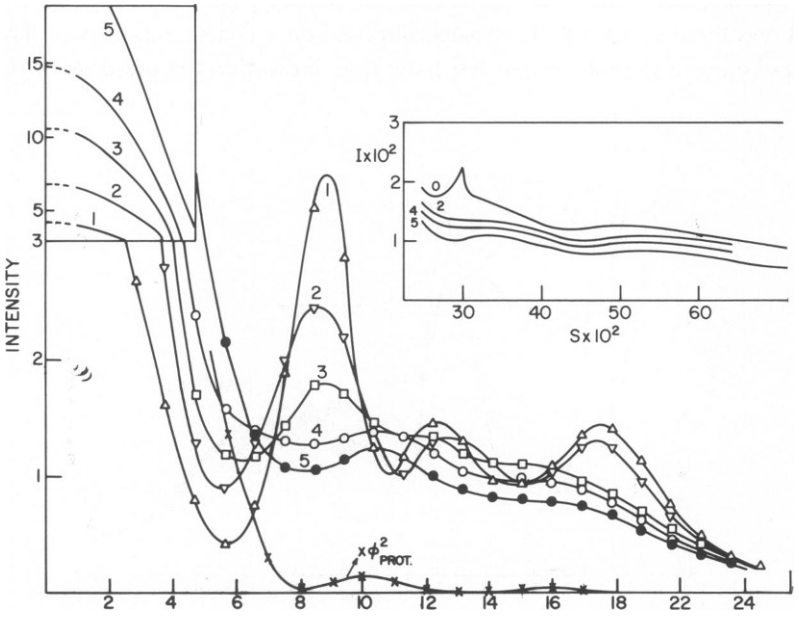

FIGURE 4 The desmeared experimental data. The abscissa is $s = (4\pi/\lambda)\sin\theta \times 10^2$. The $x\phi^2_{prot}$ curve is for the 35% protein sample.

result could be consistent with a small amount of scattering with a negative slope character, but the magnitude is not comparable to that observed even in the 6% curve (as noted, the unsmeared 0% curve goes negative in this region). Starting at 6% protein, this added intensity increases with increasing protein. At the two highest concentrations, a secondary maximum is evident at $s \simeq 0.10$, followed by a faint, broad band at $s \simeq 0.17$. At the lower concentrations, these last two contributions are negligible. But in general the predominant part of the protein scattering is concentrated to the left of $s \simeq 0.09$, conveniently isolated from the rest of the pattern.

The Fourier transforms are shown in Fig. 5. These curves give the distribution of electron pairs in the system and have been calculated, but to $r \simeq 110$ Å, a range which includes both bilayer and multilayer contributions. Features to note are the initial large peak at small r, which represents the correlation between electron densities of opposite sign. Next comes a well defined maximum at −40–45 Å, identified with the correlation of the positive electron densities of the polar head groups across the bilayer. There is then a minimum, after which a second maximum occurs at −75 Å. This latter feature becomes less prominent as the protein increases, and is very faint at the 35% concentration. It is evidently the contribution of the multilayer. A broad band is also present, increasing in magnitude with added protein and extending out to $r = 108$ Å. Clearly, the curves resolve into two domains or, $D_{ij}(r) = D_B(r) + D_m(r)$, where $D_B(r)$ ranges from 0 to ~45 Å; $D_m(r)$ overlaps $D_B(r)$ and occupies the rest of the distance range. It can be seen that the broad band contribution overlaps these two domains. With this qualitative description, we can now proceed with the identification of the contributions of the four terms of Eq. 1 to the curves of Figs. 4 and 5. We note that the ordinate of Fig. 5 is weighted by r, so that effects of any

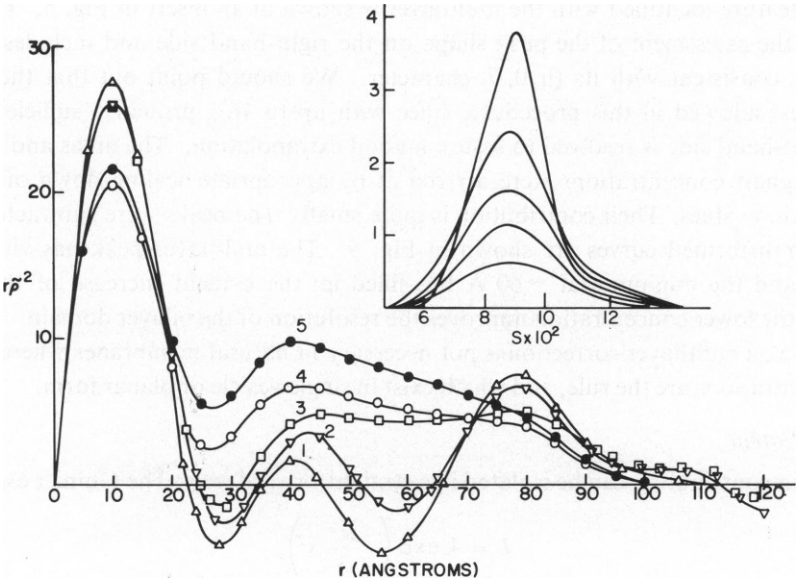

FIGURE 5 The Fourier transforms of Fig. 4. The peak at 78 Å results from the multilayer electron pair distribution. It is the transform of the multilayer peaks. The insert shows these peaks resolved in Fig. 4. See text.

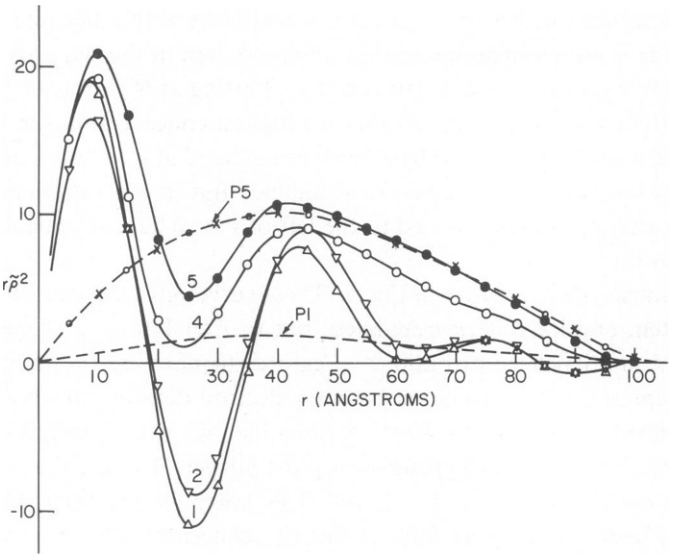

FIGURE 6 Fourier transforms of Fig. 4 after removal of the multilayer peak. The curves p_1 and p_5 are the Fourier transform of the protein scattering for the 6 and 35% protein systems, respectively. The open circles on p_5 are the points calculated from the sphere transform formula (see text).

manipulation of the curves is magnified at the larger distances. We analyze each term in order, starting with I_m.

Multilayer

The peak feature identified with the multilayer is shown in an insert in Fig. 5. The dashed portion is the assessment of the peak shape on the right-hand side and includes an asymmetric tail, consistent with its (h, 0, 0) character. We should point out that there is little arbitrariness allowed in this procedure, since with up to 16% protein a sufficient portion of the right-hand side is resolved to assure a good extrapolation. The areas and shapes for the two highest concentrations were arrived at by appropriate scaling down of the lower concentration values. Their contribution is quite small. The peaks were subtracted and the resultant transformed curves are shown in Fig. 6. The multilayer peak has virtually disappeared and the minimum at ~60 Å has filled in; the evident increase of the peak at ~44 Å in the lower concentration improves the resolution of the bilayer domain.

In general, a multilayer correction is not necessary in natural membranes where high protein concentrations are the rule, and which exist in single vesicle or planar form.

Protein

The protein contribution can be isolated in a straightforward way. The Guinier expression,

$$I = k \exp\left(-\frac{\overline{R}^2}{3} s^2\right), \tag{4}$$

for the scattering at the smallest angles is used. The radius of gyration, $\overline{R}$, is obtained from semi-logarithmic plots of the intensity against s^2. These are shown in Fig. 7. The

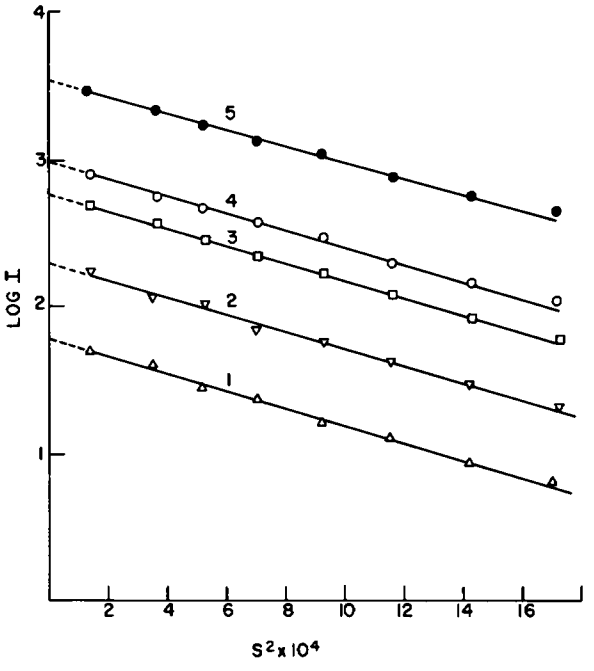

FIGURE 7 Guinier plots of the experimental data. The curves are parallel and show no interference peaks.

intensity of the pure phospholid curve in this region is very weak, with zero or negative slope. Since

$$\bar{R}^2 = \int_0^\infty r^4(\rho - \rho_0)\,d\tau \Big/ \int_0^\infty r^2(\rho - \rho_0)\,d\tau, \tag{5}$$

this means that the weighted electron density fluctuations of the negative hydrocarbon chain regions and positive polar head group regions average out to a negligible value. The protein-containing curves give straight parallel lines whose constant slope gives a value of 41.5 Å for $\bar{R}$, and whose intercepts on the ordinate are directly proportional to the protein concentration. This indicates that the protein entity in the membrane can be treated as a particle whose spatial characteristics are manifested by the shape of its scattering curve. Its morphology is identified as spherical from a plot of the spherical scattering function

$$\phi^2(sR) = \frac{9\pi}{2}\left[\frac{J_{3/2}(sR)}{(sR)^{3/2}}\right]^2, \tag{6}$$

where $R = \sqrt{5/3}\bar{R} = 54$ Å is the sphere radius. This function is shown in Fig. 4, normalized at $s = 0$ to the 35% curve, and extending over its whole effective scattering range. A Gaussian distribution of radii between ($R \pm 0.1\ R$) was assumed, mainly to indicate that the protein is not to be considered as a collection of uniform hard spheres but as an averaged set of spherically symmetric charge distributions in which significant irregularities and shape are permitted. (In fact, an axial ratio up to 1:1.3 could be allowed.) The plot fits the ex-

perimental curve over most of the small angle range; its first two maxima coincide with the two broad bands (at $s \simeq 0.10$ and 0.17) of the measured curves of Fig. 4 for both the 21 and 35% concentrations, and at least part of their intensity is contributed by the protein scattering. A final conclusion from Fig. 7 is that the linearity of the curves is a positive indication of an absence of interference effects (Brady and Gravatt, 1971) between proteins. In the context of Eq. 1, this implies a value of $C_{prot}(r) = 1$ in the protein term.

The Fourier transform of $\phi^2(sR)$ for the 35 and 6% curves are shown in Fig. 6. The sphere transform curve coincides almost perfectly with the portion of the 35% curve above ~60 Å, and this is quantitative confirmation that the broad band features of the transform curves is the protein contribution. An alternate procedure can be used to verify this. The transform of the intensity scattered by a sphere is given by the expression (Guinier, 1955):

$$rD_s(r) = r\left[1 - \frac{3}{4}\frac{r}{R} + \frac{1}{16}\left(\frac{r}{R}\right)^3 + \cdots\right].$$

By using $R = 58$ Å, this function is calculated and normalized to fit the measured curve beyond 60 Å (it also matches closely). It is then transformed and plotted in Fig. 4. A perfect fit is obtained with the measured curve at small angle and the two outer maxima again coincide with the measured ones. Thus, by either proceeding directly from the intensities, or identifying the protein contribution in the transforms and reverse transforming to obtain the intensities, the identification of the protein portion is made. This procedure is repeated for each concentration. The protein contribution is then subtracted from the curves of Fig. 6 to give Fig. 8.

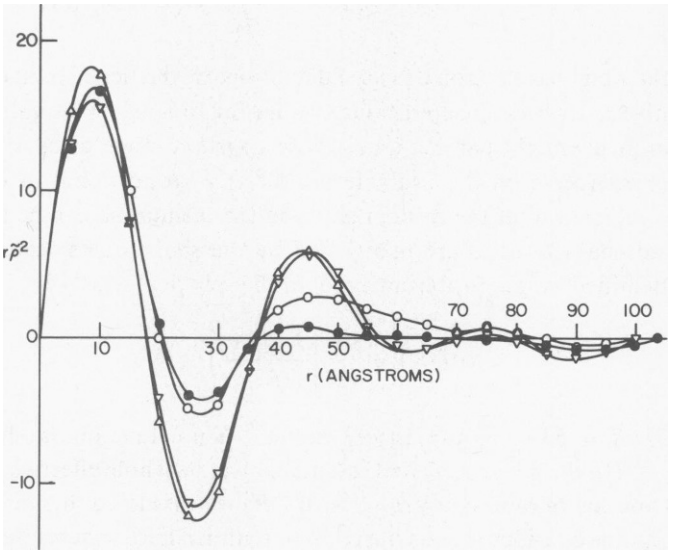

FIGURE 8 The curves of Fig. 6 after subtraction of the protein component.

The Protein-Lipid Interaction Term

The curves of Fig. 8 are the Fourier transforms of the two remaining terms $I_{lip} + I_{pl}$. We write the intensity expression for these two terms making explicit the dependence of ϕ_{lip} on x,

$$I_{lip} + I_{pl} = (1 - x)\phi_{lip}^2(s, r, x) + 2x(1 - x)\phi_{prot}(s, R)\phi_{lip}(s, r, x)C(r). \qquad (7)$$

ϕ_{prot}^2 has been determined experimentally, so ϕ_{prot}, as well as x, is known. As discussed earlier, it is the x-dependence of ϕ_{lip} that hinders the separation of the two terms. Nevertheless, the physical aspects of the I_{pl} term and its transform can be used to overcome this difficulty. The protein radius is 54 Å, so there can be no correlation terms between it and the phospholipid at distances less than this. That is, $C(r) = 0$ for $r \lesssim 54$ Å. In reciprocal s-space this implies that their major intensity contribution will lie in the range from 0 to $s \simeq [1.23(2\pi)/54] \simeq 0.14$. ϕ_{prot} is also very small above $s \simeq 0.13$ (Fig. 9). In contrast the Fourier transform of I_{lip} in Fig. 8 occupies the range from 0 to 50 Å, and thus it will lie in the range beyond $s \simeq [1.23(2\pi)/50] \simeq 0.15$. These domains are indicated in Fig. 9, where the remainder of the intensity after subtraction of I_m and I_{prot} is plotted. These curves are, of course, equivalent to the inverse Fourier transform of those of Fig. 8. The overlap region between the domains of the two terms of Eq. 7 has been split by the dashed lines. The

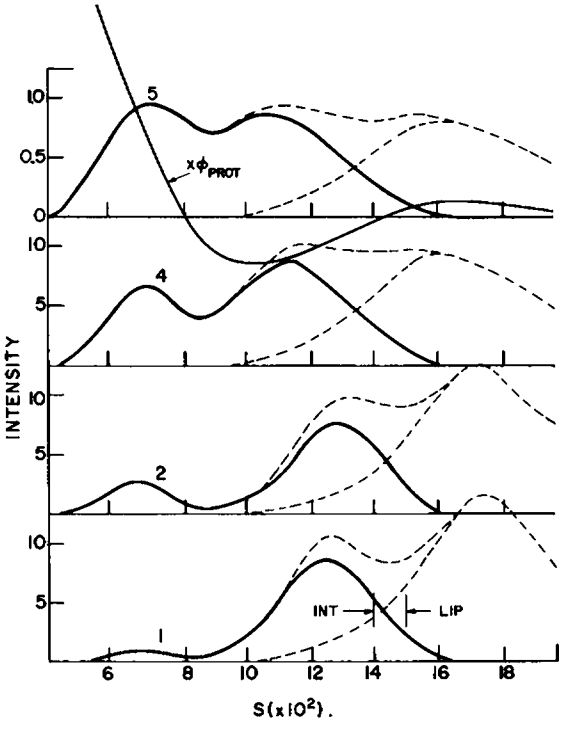

FIGURE 9 Portion of the measured intensity curves of Fig. 4 after subtraction of the multilayer and protein scattering. The end boundary of the interaction domain and the start boundary of the phospholipid domain are indicated by the vertical lines (see text).

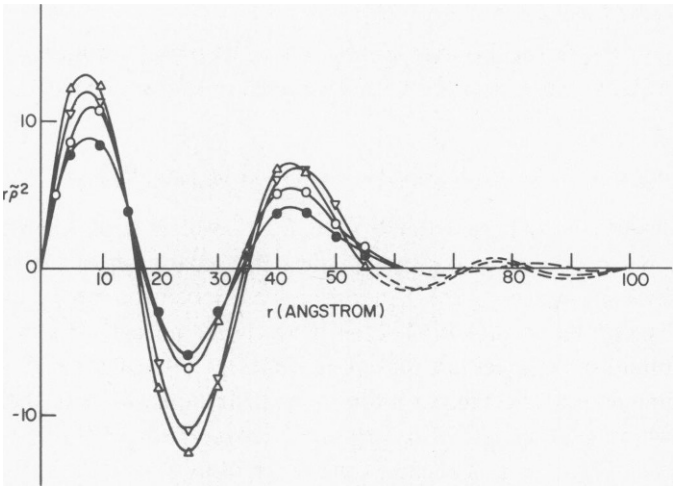

FIGURE 10 The resolved transformed phospholipid scattering. The direction r coincides with the bilayer normal.

precision with which this can be done is sensitive to any small error in the slit desmearing program that will affect the sharpness of the right-hand peak, and thus the extrapolation to zero. An error will give rise to a ripple in that region of the Fourier transform that marks the outer boundary of the bilayer domain. There can also be a series termination error due to truncation of the I_{pl} function. These errors are easily recognized and their effect on the separation evaluated by equating them to zero beyond the range of the lipid transform and inverse transforming to obtain I_{pl} (or I_{lip}) curve, whose shape in the overlap region could be compared with the original one. This was done in the evaluation of the dashed line, and the error due to ripple was found to be negligible. The resolved I_{pl} functions were then transformed and the last step in the resolution of the terms in Eq. 1 completed by subtracting them from the curves of Fig. 8. This leaves $rD_{lip}(r)$ and this function is shown in Fig. 10.

Phospholipid

The Fig. 10 curves are the electron pair distributions of the phospholipid at each protein concentration. The curves show that the introduction of protein has the effect of decreasing the magnitude of the minimum, relative to the two maxima, but in all other respects they are similar. The conclusion is that the essential bilayer character of the phospholipid phase is not changed in any drastic way. This is in agreement with the wide-angle studies (Brady & Fein, 1977). In particular, it is reasonable to conclude that the bilayer symmetry is preserved; in this case the modified Pape procedure is valid, and the pair distributions can be deconvoluted directly to give the $\rho(r)$'s. The results are shown in Fig. 11. The curves show the two maxima at a distance of $\sim$42 Å, with a negative trough between, and are similar to the curves for egg lecithin obtained by Levine and Wilkins (1971). The electron densities in the middle region are lower, however, reflecting the fact that subtraction of the protein contribution has in effect left regions of zero electron density in the membrane interior. The real electron density profile will be a composite of the densities along normals passing through

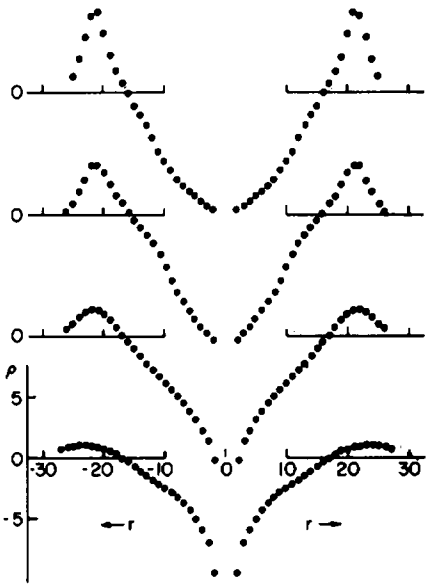

FIGURE 11 The phospholipid bilayer electron density profiles obtained by deconvoluting the curves of Fig. 10. There were Fourier series oscillations at the center and outer boundaries of the bilayer, and the data in these regions have been omitted.

both protein and lipid regions and can only be evaluated after the location of the protein in the bilayer is determined.

The Interaction Term

Before further analyzing this term, it is worthwhile now to describe briefly how its resolution is presently being improved, by electron density contrast methods. If, in a solvent of electron density ρ_0, we denote the effective electron densities of protein, polar head group, and hydrocarbon regions by $(\rho_1 - \rho_0)$, $(\rho_2 - \rho_0)$, and $(\rho_3 - \rho_0)$, and the corresponding pair correlation functions by C_{12} and C_{13}, the appropriate pair distributions for the interaction are

$$D_{12}(r) + D_{13}(r) = (\rho_1 - \rho_0)(\rho_2 - \rho_0)\bar{v}_1\bar{v}_2C_{12}(r) + (\rho_1 - \rho_0)(\rho_3 - \rho_0)\bar{v}_1\bar{v}_3C_{13}(r),$$

where v_1, v_2, and v_3 are the partial volumes. These terms are directly obtained by Fourier transformation of the terms $I_{12} = (\rho_1 - \rho_0)(\rho_2 - \rho_0)v_1v_2\int_0^\infty C_{12}(r)4\pi r^2(\sin sr/sr)\,dr$ and $I_{13} = (\rho_1 - \rho_0)(\rho_3 - \rho_0)\bar{v}_1\bar{v}_3\int_0^\infty C_{13}(r)4\pi r^2(\sin sr/sr)\,dr$. What has been isolated in Fig. 8 is $I_{12} + I_{13}$. The equations show explicitly how measurements at two different ρ_0's will serve to separate these two quantities, and, in fact, a set of experiments at six different ρ_0's allows separation of I_{11}, I_{22}, I_{33}, and I_{12} also, and is an alternative way of doing what we have just done by the concentration variation method. Separating I_{12} from I_{13} raises the resolution by another level of detail, after which a suitable computer program can justifiably be used to synthesize an exact fit of the interference terms from detailed models. This operation is essentially equivalent to using the correlation functions C_{12} and C_{13} to determine how the isolated lipid and protein structures intercalate to produce the final

membrane structure. We concentrate for now on the data of Fig. 9 that, even in their present form, provide the basis for a semi-quantitative calculation, from which the most probable location of the protein can be determined. The calculation also illustrates the genesis of the interaction term. The striking features of Fig. 9 are the double peaks, with the magnitude of the left-hand one, at $s \simeq 0.06$, increasing markedly with concentration. The right-hand one, at $s \simeq 0.125$, is displaced to the left at the higher concentrations. There is evident peak broadening in the upper curves. The shift and broadening are to be expected from the increased long-range disorder resulting from protein incorporation and will be regarded as second-order effects. Our calculation will be concerned with reproducing the double-peak character and concentration dependence of I_{pl}. We set up electron pair distribution functions for a protein imbedded in the bilayer (case 1) and for one held on the surface (case 2). These two configurations are sketched in Fig. 12. Also to be taken into account is the possible formation of a shell of phospholipid molecules around that portion of the protein surface not imbedded in the bilayer (case 1*a*). Anticipating the results, we mention here that inclusion of this configuration will affect only the magnitude of the results, but we take account of it, partly on plausibility grounds, but also because, as noted above, the phospholipid electron density in the middle is less than would be expected for an all-hydrocarbon interior; in addition, the bilayer thickness shows a gradual increase with added protein, both consistent with a forcing apart of the bilayer halves, to accommodate the inserted protein. Further, the number of (C, C) interchain distances calculated from wide-angle studies on the interchain peak profiles (Brady and Fein, 1977) shows values consistently less than those attributable to the relative decrease in phospholipid at the various protein concentrations. This is clearly an effect of (and in) the protein surface region and it does not seem justified to ignore the contribution of a configuration such as case 1*a* to it, since more than half the sur-

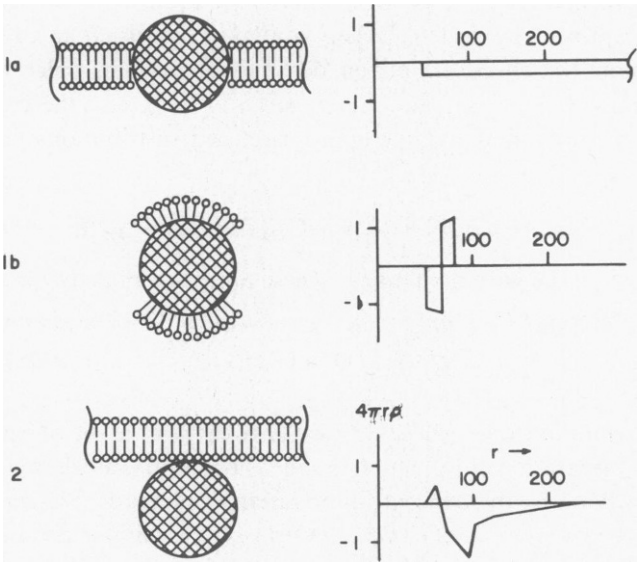

FIGURE 12 Models of an internally and externally placed protein. The electron pair distributions corresponding to each configuration are shown on the right.

face of the imbedded protein protrudes from the bilayer. In fact, the hydrocarbon ends in this orientation could be partly solubilized in the protein, accounting for the observed decrease in the number of interchain distances.

Although ϕ_{lip} is not known experimentally, we can still use the formulation of I_{pl} as a product of the scattering factors modulated by a correlation term. Instead of ϕ_{lip}, we choose an element of volume dv_i and scattering factor $\rho_i dv$ in the phospholipid; the interaction can then be written in terms of ϕ_{prot} and $\rho_i dv$, integrated over the appropriate volumes. The appropriate term for the interaction in the Debye equation (Debye, 1927) can then be written as $I = (\rho_1 - \rho)\bar{v}_1 \phi_{prot} \int_0^\infty \sum_{i=2,3} \bar{v}_i(\rho_i - \rho_0)G_i(r)(\sin sr_i/sr_i)dv_i$; $I = (\rho_1 - \rho_0)v_1 \phi_{prot} \int_0^\infty \sum_{i=2,3} 4\pi r_i^2(\rho_i - \rho_0)G_i(r)(\sin sr_i/sr_i)dr_i$, where $i = 2,3$ refers to a volume element in the polar and hydrocarbon region, respectively. The integration is along any radial direction passing through the protein center. The values of ρ_2, ρ_3, and ρ_0 are 0.385, 0.270 and 0.33 electrons/Å^3, respectively, and $G_i(r)$ will be 0 for $r \leq R_{prot}$, where R_{prot} = 54 Å. The values of $4\pi r^2 \rho G(r)$ were evaluated graphically for each configuration and are plotted on the right in Fig. 12. The units of $G(r)$ were chosen such that $G_i(r)$ was unity in the lipid, and the value of $4\pi r^2 G_i(r)$ was then that segment of the sphere intercepted by the phospholipid regions at each value of r. The upper limit of integration was 80 Å for case 1*a* (R_{prot} + ½ bilayer thickness), and 250 Å for cases 1 and 2, a value safely beyond the convergence limit of their integrals. The integrals were evaluated on the computer.

The results are shown in Fig. 13. It is seen that the double peak profile of the experimental curve is reproduced. For case 1, the maxima of both peaks coincide with the measured ones, and the concentration dependence of the left-hand one is reproduced at all concentrations. Only part of the right-hand peak area is accounted for, although the agreement becomes much better at the higher concentrations. Case 2, on the other hand, gives a profile lying in an s range too far to the left of the experimental one to be seriously considered as a possibility. Thus, the placement of the protein at the interior of the double layer is indicated by the experiments. The freeze-fracture micrographs of course agree with this finding.

The discrepancy in the right-hand peak area can be rationalized by noting that two additional effects have not been considered. The first of these is the effect on the multilayer spacing of the insertion of protein. Qualitatively, this would produce a bulge in the bilayer in this region, with the effect of decreasing the distance between its phospholipid layers and those of adjacent bilayers. This possibility is considered because the discrepancy becomes less at higher protein, where the multilayer component has been markedly reduced. The second is the effect on the phospholipid scattering of the gap (or hole) produced in the (previously) continuous bilayer by the protein. In diffraction terms, this could be regarded in terms of an equivalent process of displacing the scattering center of one region of membrane by a distance of 108 Å (= D_{prot}) relative to the other. This would introduce an interference function $\alpha(s, x, D_{prot})$ into the phospholipid scattering function ϕ_{lip}^2. Thus, $I_{lip} = (1 - x) \cdot \phi_{lip}^2 [1 + \alpha(s, x, D_{prot})]$, where in an ideal case $\rho(s, x, D_{prot})$ would increase with x to counterbalance the decrease brought about by the coefficient $(1 - x)$. Fig. 9 indicates that this gap effect would be relatively small, although not negligible. The total magnitude of the two cannot be estimated from the data presently available, but it is more than speculation to assume that they could account for the discrepancy, since their effects would occur in just this region of the scattering pattern.

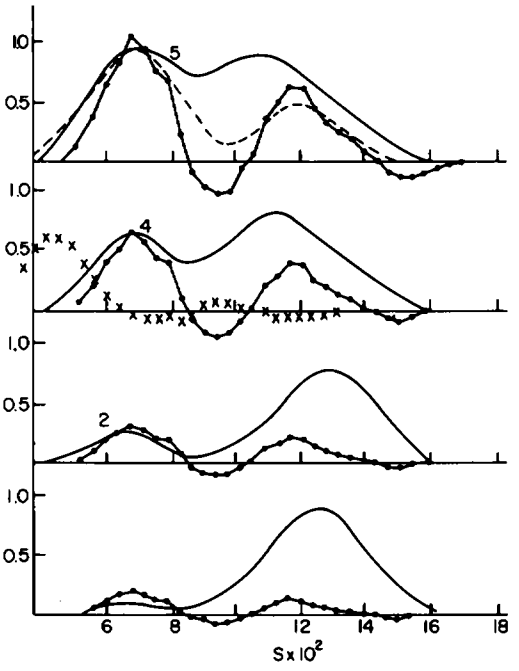

FIGURE 13 Comparison between the measured and calculated interaction term. The dots are the calculated data for a protein situated at the interior of the bilayer, and the crosses are for an externally placed protein. The curves were roughly normalized at the position of the left-hand maximum of curve 5. The dashed curve is the result of smoothing and broadening the peaks to roughly match the widths of the experimentally determined ones.

CONCLUSION

The analysis can be completed by adding the deconvoluted $\tilde{\rho}^2(r)$ of the protein, placed symmetrically at the bilayer center, to the electron density profiles of Fig. 11, to give the true profiles. Fig. 14 shows the profiles, with the protein contribution spanning the bilayer, and filling in the minimum between the polar head group regions. The calculation of the interference term illustrates that a proper deconvolution should only be made when the interaction terms are accounted for. With respect to the protein, our results clearly identify it in this case with the continuous (background) scattering, and a generalization to other systems would be that this portion of the intensity has to be taken into account in all membrane work, particularly when absolute intensities are being used.

It will be rewarding to extend this technique to natural membranes. These have the advantage of being in single bilayer vesicle or planar form, thus obviating the necessity of a multilayer correction, and offer the added challenge that the protein shape can depart widely from the spherical, thus requiring a more exhaustive exercise in the isolation and analysis of the protein term. Of particular interest is the sarcoplasmic reticulum system, in which the protein-lipid ratio can be varied and in which the protein distribution is suspected of being placed asymmetrically in the membrane. Experiments on this system are underway. A future publication will present a more complete theoretical and experimental

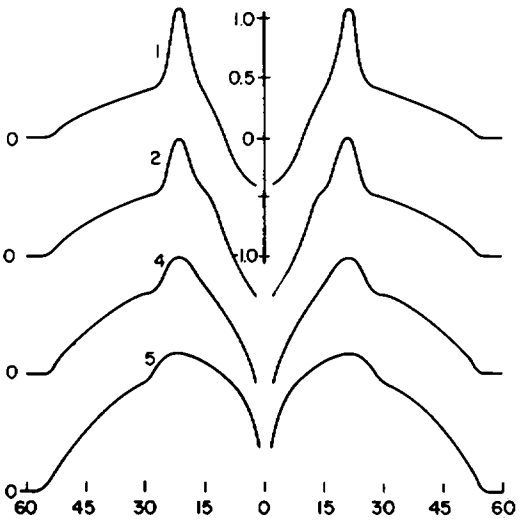

FIGURE 14 The final bilayer profiles. The deconvoluted protein transforms have been added to the phospholipid p's.

analysis of the interaction term then that presented above. Improvement in the slit desmearing procedure will result from the use in subsequent work of a two-pinhole apparatus with a 1-m scattering radius, in conjunction with a position-sensitive detector.

We would like to thank Dr. J. M. Boggs, Sick Children's Hospital, Toronto, Ontario, for preparing the membrane samples. Dr. W. J. Vail, University of Guelph, Ontario, took the electron micrographs. D. B. Fein, New York State Department of Health, contributed in many technical aspects of the research.

This work was supported by a grant from the National Science Foundation (PCM 76 07569).

Received for publication 15 August 1978 and in revised form 22 November 1978.

REFERENCES

BARTLETT, G. R. 1959. Colorimetric assay for free and phosphorylated glyceric acids. *J. Biol. Chem.* **234**:469–471.

BLASIE, J. K., M. ERECINSKA, J. S. LEIGH, and S. SAMUELS. 1977. Structure of cytochrome oxidase. Lipid Model membrane. *Biophys. J.* **17**:63*a*. (Abstr.).

BLAUROCK, A. E. 1975. Bacteriohodopsin: trans-membrane pump containing alpha-helix. *J. Mol. Biol.* **93**: 139–158.

BLAUROCK, A. E., and W. STOCKENIUS. 1971. Structure of purple membrane. *Nat. (New Biol.).* **233**:152–154.

BOGGS, J. M., W. J. VAIL, and M. A. MOSCARELLO. 1976. Preparation and properties of vesicles of purified myelin hydrophobic protein and phospholipid. A spin label study. *Biochim. Biophys. Acta.* **448**:517–530.

BRADY, G. W. 1960. Structure in ionic solutions III. *J. Chem. Phys.* **28**:1079–1082.

BRADY, G. W. 1971. Some aspects of small angle X-ray scattering. *Acc. Chem. Res.* **4**:367–373.

BRADY, G. W. 1974. On the aggregation of mixtures of long and short chain molecules. *J. Chem. Phys.* **60**:3466–3473.

BRADY, G. W., and D. B. Fein. 1977. An analysis of the X-ray interchain peak profile in dipalmitoylglycerophosphocholine. *Biochim. Biophys. Acta.* **464**:249–259.

BRADY, G. W., and D. B. FEIN. 1979. The effect of added protein on the interchain X-ray peak profile in egg lecithin. *Biophys. J.* **25**:43–47.

BRADY, G. W., and C. C. GRAVATT. 1971. Determination of the radial distribution function and the direct-correlation function of spheres by X-ray small angle scattering. *J. Chem. Phys.* **55**:5095–5101.

BRADY, G. W., and N. L. KAPLAN. 1973. Superstructure in dissolved long chains. *J. Chem. Phys.* **58**:3535–3541.

BRADY, G. W., and J. T. KRAUSE. 1957. Structure in ionic solutions I. *J. Chem. Phys.* **27**:304–308.

BRANTON, D. 1963. *Proc. Natl. Acad. Sci. U.S.A.* **50**:1071–1080.

CASPAR, D. D., and D. A. KIRSCHNER. 1971. Myelin membrane structure at 10 Å resolution. *Nat. (New Biol.).* **231**:46–55.

DEBYE, P. 1925. Note on the scattering of X-rays. *J. Math. Phys.* **4**:133–147.

ENGELMAN, D. M. 1971. Lipid bilayer structure in the membrane of *Mycoplasma laidlowii*. *J. Mol. Biol.* **58**: 153–165.

FERNANDEZ-MORAN, H. 1962. Cell membrane ultrastructure: low temperature electron microscopy studies of lipoprotein components in lamellar systems. *Res. Publ. Assoc. Res. Nerv. Ment. Dis.* V. **40**:235–267.

GAGNON, J., P. R. FINCH, D. D. WOOD, and M. A. MOSCARELLO. 1971. Isolation of a highly purified myelin protein. *Biochemistry.* **10**:4756–4760.

GUINIER, A. 1955. Small Angle Scattering of X-Rays. John Wiley & Inc., New York. 268 pp.

HENDERSON, R. 1975. Structure of purple membrane from *Halobacterium halobium*. Analysis of X-ray diffraction pattern. *J. Mol. Biol.* **93**:123–138.

HOSEMANN, R., and S. N. BAGCHI. 1962. Direct Analysis of Diffraction by Matter. North-Holland Publishing Company, Amsterdam. 734.

LESSLAUER, W., and J. K. Blasie. 1972. Direct determination of the structure of barium stearate multilayers by X-ray diffraction. *Biophys. J.* **12**:175–190.

LEVINE, Y. K., and M. H. F. WILKINS. 1971. Structure of oriented lipid bilayers. *Nat. New Biol.* **230**:69–72.

LOWDEN, J. A., M. A. MOSCARELLO, and R. MORECKI. 1966. The isolation and characterization of an acid soluble protein from myelin. *Can. J. Biochem.* **44**:567–583.

MOSCARELLO, M. A., J. GAGNON, D. D. WOOD, J. ANTHONY, and R. EPAND. 1973. Conformational flexibility of a myelin protein. *Biochemistry.* **12**:3402–3406.

PAPAHADJOPOULOS, D., M. MOSCARELLO, E. H. EYLAR, and T. ISAC. 1975*a*. Effects of proteins on thermotropic phase transitions of phospholipid membranes. *Biochim. Biophys. Acta.* **401**:317–335.

PAPAHADJOPOULOS, D., W. J. VAIL, and M. MOSCARELLO. 1975*b*. Interaction of a purified hydrophobic protein from myelin with phospholipid membranes. *J. Membr. Biol.* **22**:143–164.

PAPE, E. H., W. MENKE, D. WEICK, and R. HOSEMANN. 1974. Small angle scattering of the thylakoid membranes of *Rhodopseudomonas spheroides* in Aqueous suspensions. *Biophys. J.* **14**:221–232.

ROBERTSON, J. D. 1967. Molecular Organization and Biological Function. J. M. Allen, editor. Harper & Row, Publishers, Inc., New York. 65.

RUBEN, G. C., J. N. TELFORD, and R. C. CARROL. 1976. Identification and transmembranous localization of active cytochrome-oxidase in reconstituted membranes of purified phospholipids by electron microscopy. *J. Cell. Biol.* **68**:724–739.

SCHMIDT, P. W., and R. HIGHT, JR. 1960. Slit height corrections in small angle X-ray scattering. *Acta. Crystallogr. Sect. B. Struct. Crystallogr. Cryst. Chem.* **13**:480–496.

SCHMITT, F. O., R. S. BEAR, and G. L. CLARK. 1935. X-ray diffraction studies on nerve. *Radiology.* **25**:131–151.

SHIPLEY, G. G. 1973. Biological Membranes. D. Chapman and D. H. F. Wallach, editors. Academic Press, New York. 1.

VAIL, W. J., D. PAPAHADJOPOULOS, and M. A. MOSCARELLO. 1974. Interaction of a hydrophobic protein with liposomes. *Biochim. Biophys. Acta.* **345**:463–475.

VANDERKOOI, J., and D. E. GREEN. 1970. Biological membrane structure I: protein crystal model. *Proc. Natl. Acad. Sci. U.S.A.* **66**:615–624.

WHITE, S. H. 1976. Lipid bilayer as a solvent for small hydrophobic molecules. *Nature (Lond.).* **262**:421–422.

WHITE, S. H., D. C. PETERSON, S. SIMON, and M. MASAOYAFUSE. 1976. Formation of planar bilayer membranes from lipid monolayers. Critique. *Biophys. J.* **16**:481–489.

WILKINS, M. H. F., and A. E. BLAUROCK. 1971. Bilayer structure in membranes. *Nat. (New Biol.).* **230**:72–75.

WORTHINGTON, C. R. and A. E. BLAUROCK. 1968. Electron density model for nerve myelin. *Nature (Lond.).* **218**:87–90.

WORTHINGTON, C. R., and T. J. MCINTOSH. 1974. Direct determination of structure of peripheral nerve myelin at moderate resolution. *Biophys. J.* **14**:703–709.